Asymmetric vertical internal wave propagation

Hans van Haren[1]

Received 15 December 2005; revised 15 February 2006; accepted 22 February 2006; published 31 March 2006.

[1] Yearlong data from a single ADCP above the northern extension of the Mid-Atlantic Ridge are used to investigate vertical internal wave propagation in the open ocean (395–1025 m). Whilst 80% of incoherent semidiurnal tidal (D_2) phase propagates downward, 90% of near-inertial (f) phase propagates upward. Most upward propagating f-phase is found at sub-f frequencies $\sigma_{min}(N = f) \approx 0.74f < \sigma \leq 0.99f$, N the buoyancy frequency and σ_{min} the lower bound of the inertio-gravity (IG) wave band following the 'non-traditional approach', which includes the horizontal component of the Earth's rotation in momentum equations. The upper bound of mostly downward propagating D_2-phase coincides with the upper IG-bound $\sigma_{max}(N = f) \approx 1.35f$. The limited band $[\sigma_{min}, \sigma_{max}]$ demonstrates that f and D_2 contain special internal waves concerning vertical propagation. It is suggested that this is partially attributable to small-scale step layering in N, with N = f separating 'trapping' from 'classic propagating' wave regimes, rendering the mean large-scale N ≈ 18f less important. **Citation:** van Haren, H. (2006), Asymmetric vertical internal wave propagation, *Geophys. Res. Lett.*, *33*, L06618, doi:10.1029/2005GL025499.

1. Introduction

[2] Breaking internal waves are considered one of the most important mechanisms for mixing in the open ocean [e.g., *Gregg*, 1987]. However, details of internal wave induced mixing are not yet well understood. In particular, the variability with time, dominant frequencies, typical vertical length scales and details of (vertical) propagation of the motions that cause the (shear induced) mixing are not well known, including propagation through homogeneous layers. Most energetic internal wave motions (and shear) are at semidiurnal (subscript 2) tidal frequencies (here indicated as D_2 when no specific, lunar (M_2), solar (S_2), or other constituent is meant), mainly generated above topography like the upper continental slope in the Bay of Biscay [*Pingree and New*, 1991], and at near-inertial frequencies (f), generated via geostrophic adjustment, locally in the deep or near the surface following atmospheric disturbances, e.g., in the Mediterranean Sea, also in deep homogeneous layers where buoyancy frequency N ≈ 0 < f [*van Haren and Millot*, 2004].

[3] Focusing on f-motions, *Leaman and Sanford* [1975] suggest relatively short vertical scales O(100 m), with a strong asymmetry in propagation in their 4 day time series: they estimated ~90% of f-energy to propagate downward. Note that their frequency resolution is quite coarse with a fundamental bandwidth of only fbw ~ 0.25 cpd (cycles per day). This strong vertical asymmetry suggests f-motions generation near the surface (for N > f) but also strong absorption before they reach the sea floor. O(100 m) scales are also reported for 2 weeks time series (fbw ~ 0.07 cpd) by *Pinkel* [1983].

[4] Although these short-term observations are quite clear-cut, it remains unexplained how f-motions propagate vertically through O(1–100 m) homogeneous (neutrally density stratified) layers that exist, for example following a double-diffusive process, and how they become absorbed. A possible means for asymmetric vertical propagation is their trapping by low-frequency vorticity modifying the wave-guide when N > f [e.g., *Kunze*, 1985; *Davies and Xing*, 2004]. However, one has to consider the entire inertio-gravity (IG) wave band for propagation of free gyroscopic f-waves in a homogeneous medium in a rotating frame of reference.

[5] In this paper, observational details are presented of vertical f and D_2 IG wave propagation using yearlong 75 kHz ADCP (acoustic Doppler current profiler) data from a single mooring above Reykjanes Ridge, the Mid-Atlantic Ridge extension in the Irminger Sea, east of Greenland. The yearlong record allows high frequency resolution (fbw ~ 0.003 cpd) and detailed study of temporal variability. The focus is on the entire IG wave band, because previous deep-ocean observations showed wave-guide modifications <10% [*van Haren*, 2004b]. Only in extremely strong low-frequency vorticity areas like Kurushio Current, planetary f can be modified to f_{mod} = [0.5, 2]f [*Rainville and Pinkel*, 2004].

2. Vertical IG Wave Propagation

[6] In a vertically (in situ) density (ρ) stratified ocean, $N = (-g/\rho \cdot \partial\rho/\partial z - g^2/c_s^2)^{1/2}$, where z denotes the vertical coordinate, g acceleration of gravity and c_s speed of sound, free internal waves exist at frequencies in the range $f < \sigma < N$, following the traditional approximation, where $f = 2\Omega\sin\varphi$ the local vertical component of the Earth's rotational vector Ω at latitude φ.

[7] In a non-traditional approach, retaining also the horizontal component $f_h = 2\Omega\cos\varphi$, IG waves can be computed under an f-plane approximation, assuming energy propagates along characteristics $\xi_\pm = \mu_\pm\chi - z$ in a plane (χ, z), where the horizontal coordinate $\chi = x\cos\alpha + y\sin\alpha$, α angle to East, so that [*Badulin et al.*, 1991; *Gerkema and Shrira*, 2005a, hereinafter referred to as GSa],

$$\mu_\pm = \frac{f f_s \pm \left(f^2 f_s^2 + (\sigma^2 - f^2)\left(N^2 - \sigma^2 + f_s^2\right)\right)^{1/2}}{N^2 - \sigma^2 + f_s^2} = -\cot\theta, \quad (1)$$

where $f_s = f_h\sin\alpha$ and θ the wave vector (**k**) angle in the (χ, z)-plane: $\mathbf{k} = (k_h, m) = \kappa(\cos\theta, \sin\theta)$, k_h and m denoting

[1]Royal Netherlands Institute for Sea Research, Den Burg, The Netherlands.

0094-8276/06/2005GL025499$05.00

Table 1. Inertio-Gravity Wave Propagation Characteristics Using (1)–(3)

Condition	'Classic Propagating' σ-Range[a] ($\xi_\pm$ Opposite in z)[b]	'Trapping' σ-Range ($\xi_\pm$ Same Sign in z)[c]	Relation[d] **k** - $\xi_\pm$ ($\forall\alpha$)	Limit N	Wave "Type"
$A < 0$, $\sigma \geq f$		$f \leq \sigma < \sigma_{max}$	ambiguous	$N_{max} = f$	inertio
$A < 0$, $\sigma \leq f$	$\mathbf{(N^2 + f_s^2)^{1/2} < \sigma} \leq f$[e]		same sign in z	$N_{max} = f$	inertio
$A > 0$, $\sigma \geq f$	$f \leq \mathbf{\sigma < (N^2 + f_s^2)^{1/2}}$		opposite in z	$N_{min} = f$	gravity
$A > 0$, $\sigma \leq f$		$\sigma_{min} < \sigma \leq f$	ambiguous	$N_{min} = f$	gravity

[a]The bold part is the condition of A translated in σ-range.
[b]ξ_+ up, ξ_- down or vice versa for particular θ.
[c]ξ_+ up, ξ_- up or both down for particular θ.
[d]Only signs in z (up or down) of phase and energy propagation are considered. Opposite in z means up implies the other down (and vice versa), whilst the same sign implies up-up or down-down. Ambiguous means all possible, depending on θ.
[e]ξ_-(f) always horizontal.

the horizontal and vertical wavenumber, respectively. The group velocity vector reads from (1) in terms of θ [GSa],

$$\mathbf{c}_g = \left(\frac{\partial\sigma}{\partial k_h}, \frac{\partial\sigma}{\partial m}\right) = (2\kappa\sigma)^{-1}\left[\left(N^2 - f^2 + f_s^2\right)\sin(2\theta) - 2ff_s\cos(2\theta)\right] \cdot (\sin\theta, -\cos\theta). \quad (2)$$

The σ-range follows from the condition that the argument of the square root in (1) is real, from which the lower and upper frequency bounds are obtained [*LeBlond and Mysak*, 1978; *Brekhovskikh and Goncharov*, 1994; GSa],

$$\sigma_{min}^2 = s - \left(s^2 - f^2N^2\right)^{1/2} < f^2$$
$$\sigma_{max}^2 = s + \left(s^2 - f^2N^2\right)^{1/2} > N^2, \quad (3)$$
$$\text{where } 2s = N^2 + f^2 + f_s^2,$$

with short-wave limits at *both* bounds [GSa]. Several wave ranges and regimes follow from (3) depending on the relative values of N, f, α. For $N \gg 2\Omega$, (3) approaches the traditional range $f < \sigma < N$ and the two solutions of (1) are identical in magnitude. These two solutions can be quite different for small N, resulting, e.g., for $\sigma > f$ in steep sloping ξ_+ with high $|\mathbf{c_g}|$ and thus low energy density E_d, and in more flat ξ_- with large E_d after reflection at flat surfaces, because $m_+/m_- = \mu_-/\mu_+$ [*Gerkema and Shrira*, 2005b; hereinafter referred to as GSb]. In the limit N = 0, $0 < \sigma \leq (f^2 + f_s^2)^{1/2}$, which contains a large sub-f fraction (except at the equator). In general, the three free wave ranges sub-f $\sigma < f$, inertial $\sigma = f$ and super-f $\sigma > f$ distinguish the amount of vertical asymmetry between the $\xi_\pm$ and specific relations with phase propagation. Depending on the sign of denominator $A = N^2 - \sigma^2 + f_s^2$ in (1) four wave regimes are distinguished (Table 1).

[8] Under condition $A > 0$, or generally $N > f$, $\xi_\pm$ have opposite slope signs in z besides different steepness for $\sigma > f$, the 'classic' propagating gravity waves that always have phase and energy propagation opposite in z. However, an additional sub-f wave regime exists, in which $\xi_\pm$ have identical vertical slope signs (positive for pole- and upward propagation) besides different steepness, and in which waves can be trapped [GSb]. In this regime, the phase-energy relationship in z is ambiguous, which implies that during trapping energy may go up and down but phase propagation will have the same sign in z.

[9] Under condition $A < 0$, or generally $N < f$, the 'classic' propagating sub-f inertio (or 'gyroscopic') waves have phase and energy propagation in the same z-direction. Here, a super-f trapping regime can exist with positive $\xi_\pm$ for equator- and upward propagation.

[10] At $\sigma = f$ the mix of above regimes is found: horizontal ξ_- always has **k** to its left, whilst ξ_+ has opposite sign in z compared to **k** when $A > 0$, and the same sign when $A < 0$.

3. Data

[11] Table 2 gives details of the single ADCP-mooring. During the deployment cruise CTD-data showed considerable variation in N. This variation was observed at large scales using $\Delta z = 300$ m for which $N = 18 \pm 3f$, but more on smaller scales, e.g., for $\Delta z = 10$ m $N = 18 \pm 15f$ (Figure 1b, N is computed using the c_s-correction). O(1–10 m) thick layers of N = 0 are observed, also in the ADCP range.

[12] Low-frequency ($\sigma < 0.5$ cpd) motions and D_2 dominate ADCP's kinetic energy, followed by f (Figure 1a). For $\sigma > \sim 4$ cpd, noise becomes increasingly important. The 20° slant angle beams of the ADCP limit average current estimates over horizontal distances between 17–460 m, so that smaller-scale (high-frequency) motions are not well resolved. However, the larger-scale motions near f and D_2 are expected to be well resolved, considering the 8 m vertical bin size and aspect ratio of O(0.01) given typical coherent scales [*van Haren*, 2004b].

[13] To estimate a yearlong mean of vertical internal wave propagation, double fast Fourier transform is performed using detrended series of current components u (East) and v (North) for the transfer [z, t] → [m, σ]. In σ-space only

Table 2. Upward Looking RDI 75 kHz ADCP Mooring Details (1 cpd = $2\pi/86400$ s^{-1})

Property	Value
Latitude	58°48.72′N
Longitude	031°59.80′W
Waterdepth	1550 m
f, period T_f	1.7150 cpd, 14.0 h
Deployment	26/08/2003
Recovery	07/10/2004
Beam slant angle	20°
Transmission length	15 m
Instrument depth	1040 m
First bin	1026 m
# bins x bin size	80 × 8 m
Good data entire period	bins 2–74 (1018–442 m)
Ensemble period	900 s
Local stratification N(Δz = 300m)	31 ± 5 cpd

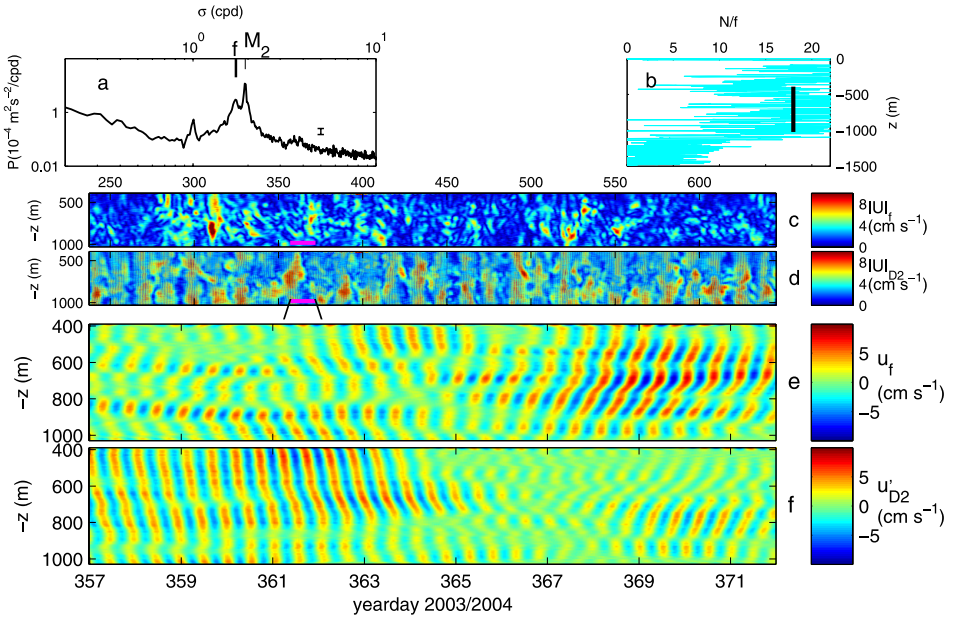

Figure 1. (a) Yearlong mean kinetic energy spectrum at 710 m. (b) N smoothed over $\Delta z = 10$ from CTD in September 2003. The black bar indicates ADCP-range at large-scale N = 18f. (c) Current amplitudes of the f-(filter: 0.85–1.07f) and (d) D_2-(0.94–1.11M_2) bands. (e) Detail for u_f and (f) u'_{D2} in which $'$ denotes incoherent part, defined relative to vertical mean: $u' = u - \langle u \rangle$. V gave similar results. Yeardays in 2004 are +365.

the amplitude^2 is retained. In m-space the positive (upward) and negative (downward) components are kept separately. This procedure establishes the vertical *phase* propagation of u and v.

4. Observations

[14] Depth-time series demonstrate strong variability of f, D_2 motions and their relative importance (Figures 1c and 1d). For D_2 the variability is overlaid with a vertical grid: large-scale coherent motions. After removal of the coherent part, these band-pass filtered data reflect 'intermittency' with time that is typical for incoherent internal waves, and more or less similar for f and D_2 [*van Haren*, 2004a]. Neither a spring-neap nor a seasonal cycle are well discernible, although enhanced $|\mathbf{U}|_f$ are found between days 300–400 and 500–550.

[15] In the vertical, mean $|\mathbf{U}|_f$ is largest between 550–850 m and $|\mathbf{U}|_{D2}$ between 850–1000 m. In time, large amplitudes occur with relatively short O(100 m) scales, with some suggestions for a dominance of downward propagation of f-energy groups and upward for D_2. However, such groups seldom start at upper and lower bounds of the ADCP range and vertical energy 'propagation' seems to be interrupted so that a characteristic does not exist of a single enhanced energy 'beam' but of energy varying between high and low (background) values.

[16] A major difference between incoherent f and D_2 is the direction of slopes of constant current component magnitude, which tend to be more sloping upward for $u(\text{or } v)_f$ and more downward for $u(\text{or } v)_{D2}$ with time (Figures 1e and 1f). Large lines are broken several (up to 10) times in the vertical by step phase changes O(10 m) thick, which can even change the sign of phase propagation in z. These scales resemble vertical scales in N (Figure 1b).

[17] The mean phase propagation determined from m, σ spectra (Figure 2) confirms the z, t observations, but informs also on sub-f and super-f. For smallest non-zero m (largest z-scale 1/m = 624 m), a sharp distinction is observed in near-f (dominant up- over downward phase propagation, with >90% of total variance upward at σ = 0.99f) compared to D_2 (80% downward at 1.01M_2). For $\sigma \geq 1.00f$ the amount of upward phase propagation decreases rapidly,

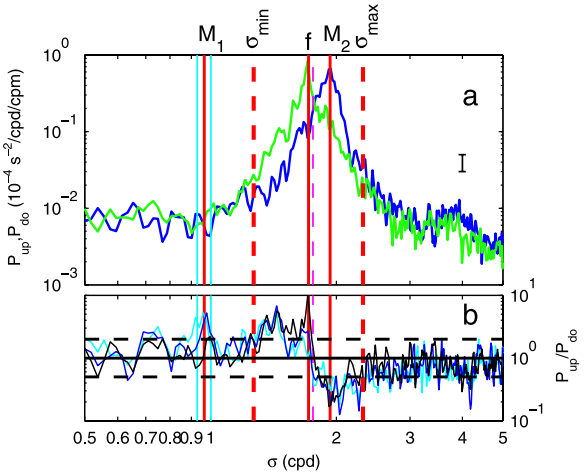

Figure 2. (a) $0.5v^2$ yearlong mean spectra of up-(green) and down-(blue) propagating phase for the second largest vertical wavelength (1/m = 312 m). (b) Spectra of up/down phase propagation ratio for 1/m = 312 (black), 208 (blue) and 156 m (light-blue), with black-dashed lines at 95% statistical significance levels. Vertical red lines indicate M_1, f and M_2, light-blue O_1 and K_1 (left-right), purple 1.025f, and red-dashed IG short wave limits (3) for N = f. Spectra for $0.5u^2$ gave similar results.

being equal to downward at $\sigma = 1.025f$, the peak frequency in other ocean areas [*Fu*, 1981; *van Haren*, 2004a]. In fact, most f-phase is propagating predominantly upward at $\sigma < f$, down to $\sigma \sim 0.75f$. Outside M_2, downward D_2 becomes less dominant and it is indistinguishable from upward at $\sigma \sim 1.35f$. These frequency bounds, designating asymmetric from symmetric vertical phase propagation, are very close to the theoretical IG short wave limits (3) for N = f: [0.74, 1.35]f.

[18] For most of this band, the ratio between up- and downward phase propagation becomes closer to 1 for higher m, but although statistical significance bounds are reached for $1/m \sim 100$ m, sub-f is always more up and super-f more down. With increasing m, energy decreases in this band (not shown), whilst a trend is found of a deviation $f \rightarrow \sigma_{min}$ for the maxima of dominant upward phase propagation and a deviation $M_2 \rightarrow S_2 \rightarrow \sigma_{max}$ for down peaks (Figure 2b). At higher m, also some significant dominant downward fourth-diurnal D_4 and upward diurnal D_1 are observed. The latter suggests some (energetically weak) sub-harmonic wave generation from D_2, at latitudes far north of the D_1-critical $|\varphi| \approx 30°$.

[19] An analysis of ADCP-data from the Bay of Biscay just below one of the largest sources of internal tide beams shows similar results, with asymmetric phase propagation limited to a band (3) for N = f(47°), except that tidal phase is dominant upward.

5. Discussion

[20] In terms of 'classic' IG wave theory for $N \gg f$, dominant upward f- and downward D_2-phase imply downward f- and upward D_2-energy propagation, provided $\sigma > f$. In principle, this is not unrealistic, given the accepted view of near-surface f-generation and D_2-generation at Reykjanes Ridge. Similarly, observations from the Bay of Biscay confirm the view of D_2-generation at the upper continental slope. However, the above would imply that little or no reflected waves are observed, just waves propagating unidirectional from their source, which seems unlikely. Furthermore, the band $[\sigma_{min}, \sigma_{max}] = [0.75, 1.35]f$ of asymmetric vertical phase propagation does contain a substantial sub-f part, which can only exist when N is small. Therefore, in the absence of large low-frequency vorticity and varying large-scale N, the observed asymmetric vertical propagation, of substantial sub-f and super-D_2 parts, needs a more elaborate explanation using the non-traditional approach in association with small-scale variations in N.

[21] Although in this approach, in contrast to the traditional approximation, 'classic' wave regimes exist that show different $\xi_{\pm}$ magnitudes and thus different wave amplitudes for weak N > f, which could explain the lack of observation of reflected waves, large-scale N = 18f is far too large and $|\xi_{\pm}|$ differ only negligibly, theoretically. Therefore, the observations are not explained solely in terms of these classic propagating wave regimes, also because IG waves cannot cross layers N = f without 'trapping' regimes.

[22] With the exception of exactly inertial waves $\sigma = f$, which are the only waves that can pass N = f (i.e., from N > f to N < f and vice versa) for $\alpha = 0$, f changes relative to σ for propagating IG waves ($\forall\alpha$). The associated change in $\xi_{\pm}$ eases transfer into the two trapping wave regimes, in which ξ_+ switch to ξ_- (or vice versa) after reflection at density or topographic surfaces. As in these regimes the sign of phase remains unaltered in z, a strong asymmetry in vertical phase propagation can be found. For example, using Table 1, a down- and poleward propagating super-f wave in N > f (A > 0) may be trapped as a sub-f wave with dominant upward phase propagation and small scales after passing at ξ_-(f) the latitude for which $\sigma = f$ [GSb]. This may explain the asymmetric (sub-)f-waves observed here. Similarly, for N < f (A < 0) a down- and equatorward sub-f wave can be trapped as a super-f wave with downward phase propagation.

[23] On the other hand, energy propagation across N = f also seems to end in trapping. For example, an up- and equatorward propagating super-f wave, initially in N > f (A > 0), may be trapped in N < f (A < 0) after reflection at $\sigma = \sigma_{max}$(N = f) and N = f layers having dominant downward phase propagation, as in the D_2-waves observed here, although a discrepancy is noted between O(100 m) z-scales of D_2 compared to O(1–10 m) of N = 0. Similarly, a down- and poleward (downward phase) propagating sub-f wave, initially in N < f (A < 0), will be trapped between N = f and $N \gg f$, for σ_{min}(N = f) < $\sigma \leq$ f (arbitrary α).

[24] The above suggests a relation between waves and small-scale variations in N, and does imply a strict separation between super-f(incl. D_2-)maxima (in N < f) and (sub-)f-maxima (in N > f) in addition to the propagating 'classic' wave regimes, with N = f bounding the 'trapping' wave regimes [f, 1.35f] and [0.74f, f], respectively. As the present observations are from a single position, vertical intermittency of wave energy could also (partly) be due to horizontal intermittency in the wave field in addition to varying N. Nonetheless, although detailed time series on N are not available, ADCP-data do indeed show a strict separation of f and D_2 in [z, t] (Figures 1e and 1f). In time in this example, $|u'|_{D2}$ is large in the first half, whilst $|u|_f$ in the second half. In the latter, the period in $|u|_f$ is ~10% larger ($\sigma <$ f) than in the first half ($\sigma >$ f). In the vertical, e.g., f-maxima are found near 600 m and between 800–900 m during days 357–364 around large D_2 between 600–800 m, whilst large D_2 is found between 750–850 m during 369–372 squeezed between layers of large f. If trapping is important, it is suggested that energy spread away from f and M_2 is associated with space-time variability in thin high-N-layers in which local generation of high-frequency waves can occur. Such waves apparently fill the spectrum up to large-scale N following advection passed the sensors and, due to their small scales, they can break occasionally.

[25] Further analysis of these data will be performed on the relation of large phase changes and, thus, large destabilizing shear with thin layers of large local N. Also, time variability including that of u,v hodographs will be analysed in detail on vertical propagation.

[26] **Acknowledgments.** I thank the crews of the R/V Pelagia (deployment) and R/V Darwin (recovery) and Hendrik van Aken for obtaining the data during LOCO-CAMP. Theo Hillebrand and MTM prepared the mooring and instrumentation. I thank Claude Millot, Theo Gerkema and Leo Maas for continuing discussions. LOCO is supported by a large-budget investment grant from NWO.

References

Badulin, S. I., V. M. Vasilenko, and M. I. Yaremchuk (1991), Interpretation of quasi-inertial motions using Megapoligon data as an example, *Izv. Atmos. Oceanic Phys.*, *27*, 446–452.

Brekhovskikh, L. M., and V. Goncharov (1994), *Mechanics of Continua and Wave Dynamics*, 342 pp., Springer, New York.

Davies, A. M., and J. Xing (2004), Wind-induced motion in the vicinity of a bottom density front: Response to forcing frequency, *J. Geophys. Res.*, *109*, C09002, doi:10.1029/2003JC002151.

Fu, L.-L. (1981), Observation and models of inertial waves in the deep ocean, *Rev. Geophys.*, *19*, 141–170.

Gerkema, T., and V. I. Shrira (2005a), Near-inertial waves in the ocean: Beyond the "traditional approximation,", *J. Fluid Mech.*, *529*, 195–219.

Gerkema, T., and V. I. Shrira (2005b), Near-inertial waves on the "non-traditional" β plane, *J. Geophys. Res.*, *110*, C01003, doi:10.1029/2004JC002519.

Gregg, M. C. (1987), Diapycnal mixing in the themocline: A review, *J. Geophys. Res.*, *92*, 5249–5286.

Kunze, E. (1985), Near-inertial wave propagation in geostrophic shear, *J. Phys. Oceanogr.*, *15*, 544–565.

Leaman, K. D., and T. B. Sanford (1975), Vertical propagation of inertial waves: A vector spectral analysis of velocity profiles, *J. Geophys. Res.*, *80*, 1975–1978.

LeBlond, P. H., and L. A. Mysak (1978), *Waves in the Ocean*, 602 pp., Elsevier, New York.

Pingree, R. D., and A. L. New (1991), Abyssal penetration and bottom reflection of internal tidal energy into the Bay of Biscay, *J. Phys. Oceanogr.*, *21*, 28–39.

Pinkel, R. (1983), Doppler sonar observations of internal waves: Wave-field structure, *J. Phys. Oceanogr.*, *13*, 804–815.

Rainville, L., and R. Pinkel (2004), Observations of energetic high-wavenumber internal waves in the Kuroshio, *J. Phys. Oceanogr.*, *34*, 1495–1505.

van Haren, H. (2004a), Bandwidth similarity at inertial and tidal frequencies in kinetic energy spectra from the Bay of Biscay, *Deep Sea Res., Part I*, *51*, 637–652.

van Haren, H. (2004b), Spatial variability of deep-ocean motions above an abyssal plain, *J. Geophys. Res.*, *109*, C12014, doi:10.1029/2004JC002558.

van Haren, H., and C. Millot (2004), Rectilinear and circular inertial motions in the western Mediterranean Sea, *Deep Sea Res., Part I*, *51*, 1441–1455.

H. van Haren, Royal Netherlands Institute for Sea Research (NIOZ), P.O. Box 59, NL-1790 AB Den Burg, The Netherlands. (hansvh@nioz.nl)